catalysts

MDPI

Article

Hydrogen Evolution Reaction of γ-$Mo_{0.5}W_{0.5}$ C Achieved by High Pressure High Temperature Synthesis

Yingfei Hu [1], Gan Jia [1], Shuailing Ma [2], Jianqiang Hu [1], Pinwen Zhu [2,*], Tian Cui [2], Zhaosheng Li [1,*] and Zhigang Zou [1,3]

1 Collaborative Innovation Center of Advanced Microstructures, National Laboratory of Solid State Microstructures, College of Engineering and Applied Sciences, Nanjing University, 22 Hankou Road, Nanjing 210093, China; huyingfei1987@163.com (Y.H.); fengxing915@sina.com (G.J.); hujianqiang_1988@163.com (J.H.); zgzou@nju.edu.cn (Z.Z.)

2 State Key Lab of Superhard Materials, College of Physics, Jilin University, 2699 Qianjin Street, Changchun 130012, China; msljlu@163.com (S.M.); cuitian@jlu.edu.cn (T.C.)

3 Jiangsu Key Laboratory for Nano Technology, Department of Physics, Nanjing University, 22 Hankou Road, Nanjing 210093, China

* Correspondence: zhupw@jlu.edu.cn (P.Z.); zsli@nju.edu.cn (Z.L.); Tel.: +86-189-4314-5826 (P.Z.); +86-25-8368-6630 (Z.L.)

Academic Editors: Di-Jia Liu and Jianguo Liu
Received: 30 October 2016; Accepted: 5 December 2016; Published: 17 December 2016

Abstract: For the first time, the hydrogen evolution reaction (HER) electrocatalytic performances of incompressible γ-$Mo_{0.5}W_{0.5}C$, prepared by high-pressure, high-temperature (HPHT) synthesis, were investigated in the electrolyte. The polarization curve of the γ-$Mo_{0.5}W_{0.5}C$ cathode exhibits the current density of 50 mA·cm^{-2} at an overpotential value of 320 mV. The corresponding Tafel slope of the incompressible γ-$Mo_{0.5}W_{0.5}C$ is 74 mV·dec^{-1}. After a 1000-cycle test, and then exposure to the air for six months, the γ-$Mo_{0.5}W_{0.5}C$ electrode performed a current density of 50 mA·cm^{-2} at an overpotential of 354 mV, which was close to the initial one.

Keywords: hydrogen evolution reaction; incompressible; high pressure high temperature synthesis; transition metal carbides

1. Introduction

As the most widely distributed substance in the universe, hydrogen is one type of clean and renewable energy resource to replace fossil fuels. Water splitting is an efficient way to produce hydrogen from an electrolyte [1–5]. The most efficient hydrogen evolution reaction (HER) electrocatalysts are Pt-group metals with extremely low overpotentials and the efficient Tafel reaction process. Considering they are scarce and expensive, substitutions are required [6–9]. Possessing similar chemical and catalytic properties to those of Pt-group metals, transition metal carbides (TMCs) have attracted a great deal of attention. The transition metal-carbon bonds are capable of changing metal-metal bond distances, downshifting the metal d-band center, and conducting substantial charge transfer from transition metals to carbons. These electronic disturbances caused by the ligand effect from carbons play an important role in the reactivity of transition metals toward hydrogen atoms [10–14].

In view of the above mentioned advantages, an increasing number of TMCs have been used in the hydrogen evolution reaction [15–18]. Recently, through the carbonization of transition metal oxides, Roman-Leshkov's group synthesized WC and β-$Mo_xW_{1-x}C$ nanoparticles performing high electrocatalytic activity and stability [19]. Wan et al. synthetized four phases of molybdenum carbide (α-MoC_{1-x}, β-Mo_2C, η-MoC, and γ-MoC), studied and compared the catalytic performances for multiple phases of molybdenum carbide [20,21].

The main synthetic methods of TMCs are as below: the direct carbonization of transition metal oxides [22], chemical vapor deposition (CVD) [23], the self-propagating high-temperature synthesis (SHS) [24], and microwave treatment [25]. Additionally, high-pressure, high-temperature (HPHT) is an effective way to prepare TMCs. The general advantages for the HPHT method are as follows: short synthesis period, a wide range of selected materials, and effectively avoiding phase segregation [26–28]. In previous work, incompressible γ-$Mo_{0.5}W_{0.5}C$ has been synthetized from the HPHT strategy, utilizing the simplest raw materials (pure Mo, W, and C) and rapidly obtained the target products (20–60 min) [29]. In this study, we explore the feasibility of this type of incompressible TMCs applied in the hydrogen evolution reaction.

2. Results and Discussion

2.1. XRD Pattern and Raman Spectrum

The crystal structure and phase of as-prepared γ-$Mo_{0.5}W_{0.5}C$ are determined by X-ray diffraction (XRD) analysis (Figure 1a). There are three primary diffraction peaks at around 31.7°, 35.7°, and 48.5°, which can be indexed as (0 0 1), (1 0 0), and (1 0 1) diffraction planes (JCPDS 65-8770). The crystal structure of γ-$Mo_{0.5}W_{0.5}C$ is shown in Figure 1b. According to the substitution of Mo atoms by W atoms in γ-MoC, γ-$Mo_{0.5}W_{0.5}C$ has the same structure as γ-MoC (hexagonal). The space group is $P\bar{6}\ m^2$ and the lattice parameters are as following: $a = b = 2.901(3)$ Å, and $c = 2.8424(5)$ Å ($\alpha = \beta = 90°$, $\gamma = 120°$). The Raman spectrum of incompressible γ-$Mo_{0.5}W_{0.5}C$ with an excitation wavelength at 532 nm is shown in Figure 2. A silicon wafer with the standard peak of 521.7 cm^{-1} was used for calibration. The characteristic Raman peaks of 908.6 cm^{-1} and 951.1 cm^{-1} are assigned to the symmetric stretching modes of Mo-Mo bonds and Mo-W bonds.

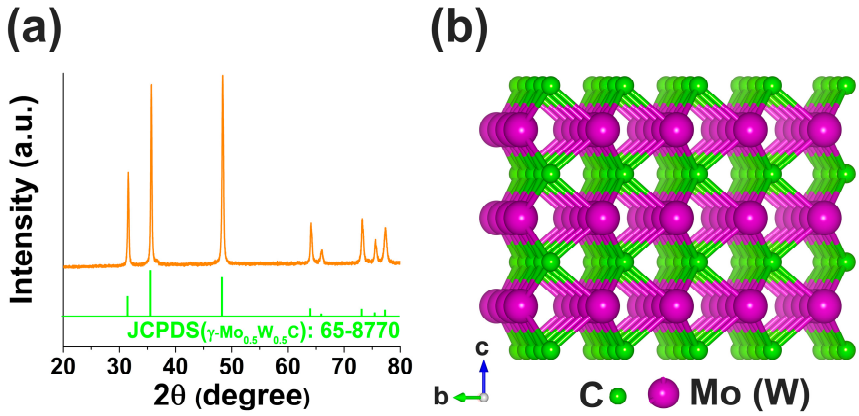

Figure 1. (**a**) X-ray diffraction (XRD) pattern and (**b**) crystal structure of γ-$Mo_{0.5}W_{0.5}C$.

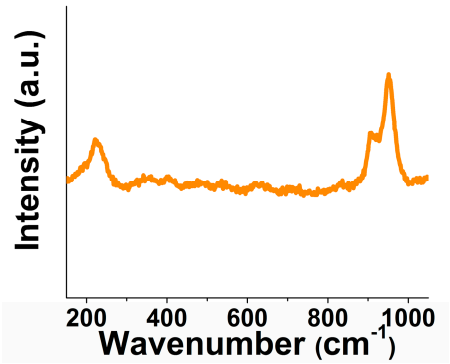

Figure 2. Raman spectrum of the γ-$Mo_{0.5}W_{0.5}C$ sample with an excitation wavelength at 532 nm.

2.2. XPS Analysis

Figure 3 shows the XPS profiles of C, Mo, and W elements, respectively. The XPS curve of 1 s electron spin-orbit of C only has a primary peak at 284.3 eV indicating that impurity substance of carbon or graphitic carbon is detected. Obviously, there are two undivided peaks for the Mo 3d electron. After dividing the peak and fitting, the first pair of peaks ($3d_{3/2}$ at 231.2 ± 0.1 eV and $3d_{5/2}$ at 228.4 ± 0.1 eV) is attributed to Mo^{4+} (Mo in MoC) or MoO_2 [30] (for this sample, they are more likely to represent Mo in MoC). The pair of small peaks ($3d_{3/2}$ at 235.3 ± 0.1 eV and $3d_{5/2}$ at 232.9 ± 0.1 eV) is assigned to Mo^{6+}. Higher valence states are very few, possibly due to the ambient graphitic carbon preventing the oxidation of Mo with low valence states. The profile of the W 4f electron shows two strong humps and a weak bulge. Through data analysis, the couple of peaks (33.7 ± 0.1 eV and 31.6 ± 0.1 eV) can be identified as characteristic peaks for WC. A small amount of higher valence state (37.6 ± 0.1 eV and 35.6 ± 0.1 eV) is also detected demonstrating the limited oxidation of the WC.

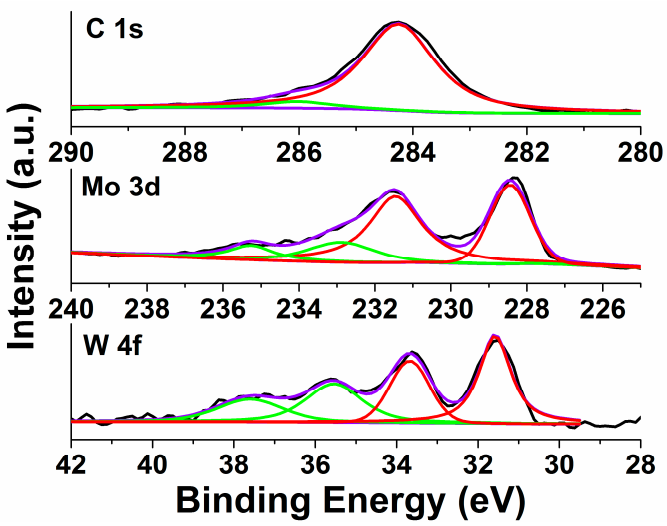

Figure 3. X-ray photoelectron spectroscopy (XPS) spectra of C 1s, Mo 3d, and W 4f in γ-$Mo_{0.5}W_{0.5}C$.

2.3. SEM, TEM, HR-TEM, and SAED Images

The surface morphology of γ-$Mo_{0.5}W_{0.5}C$ (Figure 4a) was investigated by scanning electron microscope (SEM). It is obvious that the sample displays aggregated morphologies, which are comprised of bulks and particles. Energy dispersive spectrometer (EDS) mapping of the selected area exhibits Mo, W elements distribute according to the morphology of γ-$Mo_{0.5}W_{0.5}C$ sample (Figure S1). In addition, the measured Mo/W ratio is about 1.04/1. Transmission electron microscopy (TEM) was further used to observe the morphology and microstructure of the sample. Observed by TEM, the morphology of γ-$Mo_{0.5}W_{0.5}C$ is made up of irregular bulks (Figure 4b). The analysis of high resolution transmission electron microscopy (HR-TEM) exhibits that the fringe with d = 0.191 nm matching the (1 0 1) or (0 1 $\bar{1}$) crystallographic plane of γ-$Mo_{0.5}W_{0.5}C$ (Figure 4c). The selected five diffraction spots can be indexed as the (1 1 0), (1 $\bar{1}$ 2), (1 0 1), (0 1 $\bar{1}$), and (2 0 2) crystallographic planes (Figure 4d).

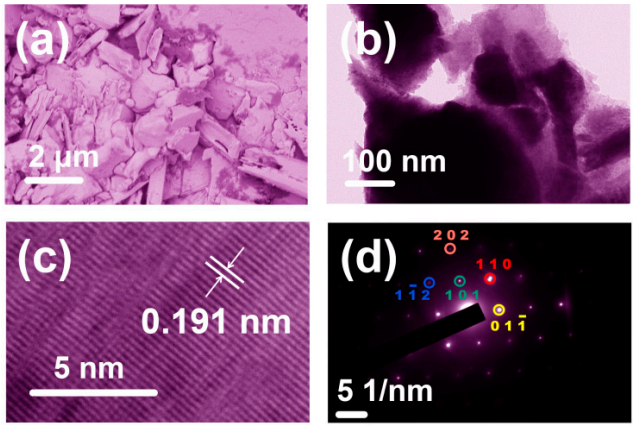

Figure 4. (**a**) Scanning electron microscope (SEM); (**b**) transmission electron microscopy (TEM); (**c**) high resolution transmission electron microscopy (HR-TEM); and (**d**) selected area electron diffraction (SAED) images of the γ-$Mo_{0.5}W_{0.5}C$ sample.

2.4. Hydrogen Evolution Reaction of the γ-$Mo_{0.5}W_{0.5}C$ Electrode

The HER activities of incompressible γ-$Mo_{0.5}W_{0.5}C$ in 0.5 M H_2SO_4 solution were investigated in the potential range between 0.2 and −0.4 V vs. reversible hydrogen electrode (RHE). As a control experiment, a commercial Pt catalyst (Pt sheet, 0.5 cm^{-2}) was also tested. Before electrochemical testing, the electrolyte was purged by hydrogen to suppress the interference of other gases. Figure 5a shows the polarization curves (*j-V* plot, iR corrected) recorded for γ-$Mo_{0.5}W_{0.5}C$ and Pt. For driving a catalytic current density of 10 mA·cm^{-2}, γ-$Mo_{0.5}W_{0.5}C$ needs an overpotential of 265 mV. To bring a current density of 50 mA·cm^{-2}, an overpotential value of 320 mV is required. According to the Tafel equation ($\eta = a + b \log(i)$, where b is the Tafel slope and i is the current density) [31], the linearization ranges of the polarization curves were fitted. The corresponding Tafel slope of the Pt was about 30 mV·dec^{-1}, which is in accord with the reported result [32]. The apparent Tafel slope of the γ-$Mo_{0.5}W_{0.5}C$ (showing a larger value of Pt) is 74 mV·dec^{-1}. HER performance of γ-$Mo_{0.5}W_{0.5}C$ in base is shown in Figure S3. The γ-$Mo_{0.5}W_{0.5}C$ cathode exhibits the catalytic current density of 10 mA·cm^{-2} at η = 283 mV. To achieve a current density of 50 mA·cm^{-2}, the cathode needs an overpotential value of 408 mV.

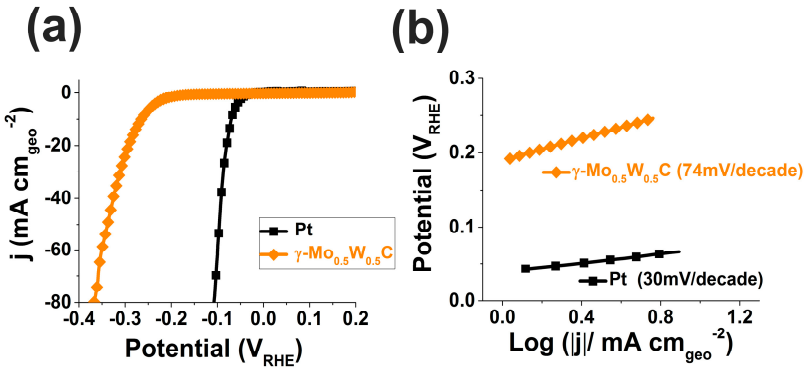

Figure 5. Electrocatalytic activities of γ-$Mo_{0.5}W_{0.5}C$ electrode in 0.5 M H_2SO_4. (**a**) Polarization curves; and (**b**) Tafel plots. The data were iR corrected.

2.5. Durability and Stability Analysis

Durability and stability are two important parameters for the catalysts during constant testing [33]. Durability of the catalytic response was detected by cycling γ-$Mo_{0.5}W_{0.5}C$ electrode continuously for

1000 cycles, shown in Figure 6. After 1000 cycles, the polarization curve of the γ-$Mo_{0.5}W_{0.5}C$ electrode exhibited an attenuation compared to the initial one (a current density of 50 mA·cm^{-2} at η = 380 mV). Then, the cathode which was exposed to the air for six months performed the catalytic current density approaching that of initial electrode (50 mA·cm^{-2} at η = 354 mV), indicating a superior durability. The stability of the γ-$Mo_{0.5}W_{0.5}C$ electrode was tested in a long-term constant potential experiment (Figure 7). During 25 h of measurement, the time-dependent current density curve was stable at ~6 mA·cm^{-2} under a static applied potential of 260 mV, demonstrating the γ-$Mo_{0.5}W_{0.5}C$ electrode can maintain its catalytic activity for a long time.

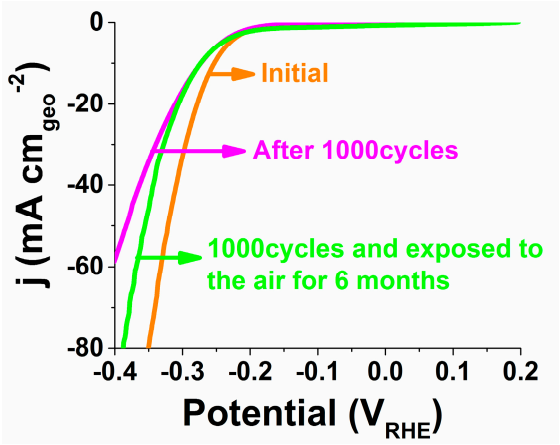

Figure 6. Polarization curves of γ-$Mo_{0.5}W_{0.5}C$ electrode before and after durability tests.

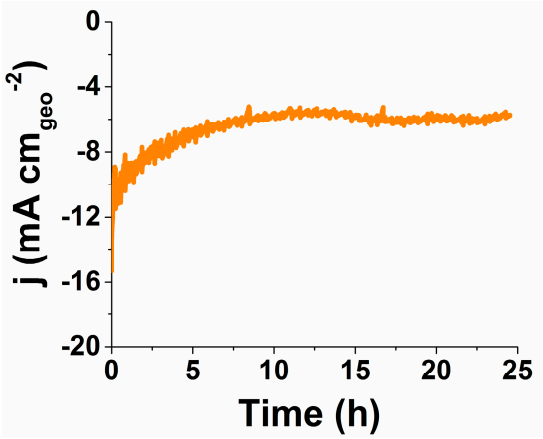

Figure 7. *I-t* curve of γ-$Mo_{0.5}W_{0.5}C$ electrode in 0.5 M H_2SO_4 under a static applied potential of 260 mV.

2.6. EIS Measurements

Electrochemical impedance spectroscopy (EIS) observations on the γ-$Mo_{0.5}W_{0.5}C$ cathode were carried out to explore the HER electrode kinetics. The Nyquist plots were exhibited at different applied overpotentials. Accompanying the increase in voltages (70–240 mV), the radii of the Nyquist arcs were weaken regularly demonstrating the charge transfer resistances of γ-$Mo_{0.5}W_{0.5}C$ were substantially reduced at higher overpotentials (Figure 8a).The data were fitted by an equivalent circuit made up primarily of a resistor (R_s) in series with two parallel circuit elements of a resistor (R_1, $R_{ct,interface}$) and a constant phase element (CPE_1, CPE_2) [34]. R_s shows the ohmic resistance from the system, R_1-CPE_1 is able to represent the interfacial resistance resulting from the electron transport in the particles of the bulk γ-$Mo_{0.5}W_{0.5}C$, and $R_{ct,interface}$-CPE_2 may relate to the charge transfer resistance at the interface between the cathode and the electrolyte. According to previous HER reports [35,36], $R_{ct,interface}$ is the

most important parameter related to electrochemical activities. The $R_{ct,interface}$ which was analyzed by equivalent circuit gradually decreased accompanying with the increase of voltage. (Figure 8b) The decreasing tendency for $R_{ct,interface}$ at various voltages are corresponding with the changes of the catalytic current density.

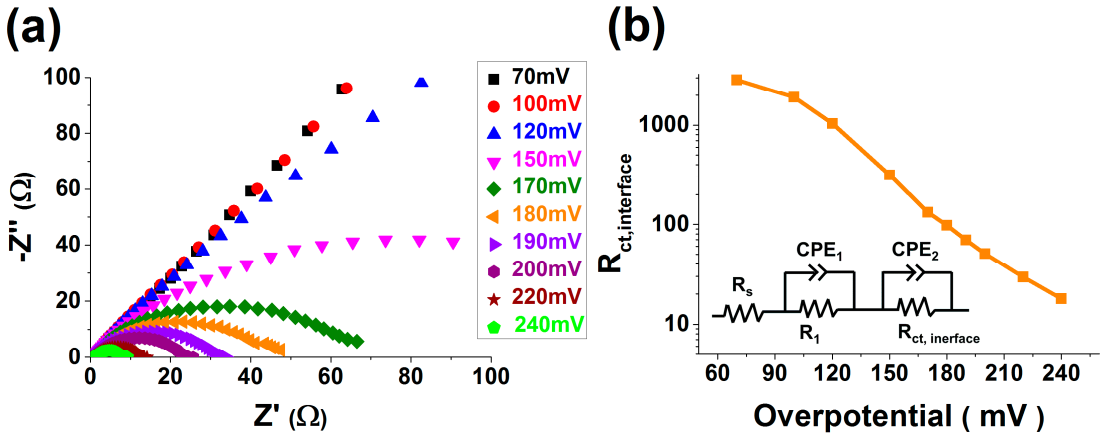

Figure 8. (**a**) The Nyquist plots of collected on γ-$Mo_{0.5}W_{0.5}C$ electrode at designated overpotentials; and (**b**) the possible equivalent circuit (insert) and the fitted values of $R_{ct,interface}$.

3. Experimental Section

3.1. Preparation of the γ-$Mo_{0.5}W_{0.5}C$ Cathode

The synthesis details of incompressible γ-$Mo_{0.5}W_{0.5}C$ were described in an earlier report [29]. Powders of pure molybdenum (99.95% in purity), tungsten (99.8% in purity), and amorphous carbon (99.5% in purity) at a ratio of 1:1:2 were mixed together in an agate mortar and pestle to obtain a uniform mixture. Then, the mixture was pressed into a cylindrical sample. A hexagonal BN capsule containing a pellet was used. By the Smart power distribution (SPD) 6 × 600 T cubic anvil equipment, the sample was heated to 2000 K at the rate of 120 $K \cdot s^{-1}$ with a pressure of 5.0 GPa, and kept at this temperature for 20 min. Then, the final sample was quenched to room temperature. The cylindrical sample was bonded with a copper rod by silver paint. The as-prepared electrode was dried in the drying cabinet to ensure the tight junction between the copper rod and γ-$Mo_{0.5}W_{0.5}C$. Finally, a plane of ~0.1 cm^{-2} was exposed and the other part of the electrode was enwrapped by the epoxide-resin glue to prevent permeation of the electrolyte. The similar methods were adopted to prepare the η-MoC (Figures S4–S6) electrode.

3.2. Electrochemical Measurement

The electrochemical properties were investigated in a conventional three-electrode cell by using electrochemical workstations (CHI-760E, Shanghai Chenhua, Shanghai, China). The prepared cathodes were adopted as the working electrode, and the counter and reference electrodes were composed of a graphite rod and an Ag/AgCl electrode, respectively. The conversion formula for a RHE potential is shown as follows: $V_{RHE} = V_{Ag/AgCl} + 0.059 \times pH + 0.197$. The electrolyte was 0.5 M H_2SO_4 (pH = 0) and 1 M NaOH (pH = 13.6) aqueous solution.

3.3. Characterization

The crystallinity and the grain size of all the samples were detected by X-ray diffraction (XRD, Rigaku Ultima III) with Cu Kα radiation (λ = 1.54056 Å). A LabRAM ARAMIS Raman spectrometer (HORIBA Scientific, Edison, NJ, USA) was used to measure the composition of material and stress state of chemical bonds. The chemical states of elements were investigated by X-ray photoelectron

spectroscopy (XPS, Thermo ESCALAB 250, UK). The morphologies of samples were surveyed by scanning electron microscopy (Zeiss Ultra 55-44-08, Pleasanton, CA, USA). High-resolution TEM (HR-TEM) and selected-area electron diffraction (SAED, Japan) were carried out through a high-resolution transmission electron microscope (JEM-2100). An electrochemical analyzer (Solartron 1260 + 1287, Farnborough, UK) was used to investigate the electrochemical impedance spectra (EIS) of the electrodes.

4. Conclusions

We demonstrated the hydrogen evolution reaction (HER) of incompressible γ-$Mo_{0.5}W_{0.5}C$ in this work. Incompressible γ-$Mo_{0.5}W_{0.5}C$ produced from the simple Mo, W, and C raw materials via the HPHT method has been researched as an efficient catalyst for HER experiments. The crystal structure and phase of as-prepared γ-$Mo_{0.5}W_{0.5}C$ are determined by X-ray diffraction (XRD) analysis. The XRD pattern of incompressible γ-$Mo_{0.5}W_{0.5}C$, the corresponding space group of which is $P\bar{6}\ m^2$, is in accord with that of the standard PDF pattern (JCPDS 65-8770). The γ-$Mo_{0.5}W_{0.5}C$ cathode exhibits the catalytic current density of 50 mA·cm^{-2} at η = 320 mV. The corresponding Tafel slope of the electrode is 74 mV·dec^{-1}. After 1000 cycles, the polarization curve of the γ-$Mo_{0.5}W_{0.5}C$ electrode exhibited an attenuation compared to the initial one (a current density of 50 mA·cm^{-2} at η = 380 mV). The time dependent current density curve was stable at ~6 mA·cm^{-2} for about 25 h under a static applied potential of 260 mV. The data of durability and stability test indicate that the electrode can maintain the catalytic activities for a long time.

Supplementary Materials: The following are available online at www.mdpi.com/2073-4344/6/12/208/s1. Figure S1: EDS mapping images of γ-$Mo_{0.5}W_{0.5}C$ sample. Figure S2: Photograph of γ-$Mo_{0.5}W_{0.5}C$ electrode collected with a hydrogen evolution reaction. Figure S3: Polarization curve of the γ-$Mo_{0.5}W_{0.5}C$ electrode in 1 M NaOH. Figure S4: XRD pattern and standard PDF data of η-MoC. Figure S5: Surface morphology of η-MoC. Figure S6: Polarization curve of the η-MoC electrode in 0.5 M H_2SO_4. The data were iR corrected. Table S1: Comparison of HER performance in acid media for γ-$Mo_{0.5}W_{0.5}C$ with other TMCs electrocatalysts.

Acknowledgments: This work was supported by National Basic Research Program of China (973 Program, 2013CB632404), a Project Funded by the Priority Academic Program Development of Jiangsu Higher Education Institutions, New Century Excellent Talents in University (NCET-12-0268), and the National Natural Science Foundation of China (21473090 and 51272102).

Author Contributions: The HER experimental work was conceived and designed by Z.L. and Z.Z.; P.Z., T.C. and S.M. synthetized incompressible γ-$Mo_{0.5}W_{0.5}C$ sample; the physical and electrochemical characterizations were executed by Y.H.; G.J. and J.H. analyzed the data; Z.L. and Y.H. drafted the paper. The manuscript was amended through the comments of all authors.

Conflicts of Interest: The authors declare no conflict of interest.

References

1. Walter, M.G.; Warren, E.L.; McKone, J.R.; Boettcher, S.W.; Mi, Q.; Santori, E.A.; Lewis, N.S. Solar water splitting cells. *Chem. Rev.* **2010**, *110*, 6446–6473. [CrossRef] [PubMed]
2. Li, Z.S.; Luo, W.J.; Zhang, M.L.; Feng, J.Y.; Zou, Z.G. Photoelectrochemical cells for solar hydrogen production: Current state of promising photoelectrodes, methods to improve their properties, and outlook. *Energy Environ. Sci.* **2013**, *6*, 347–370. [CrossRef]
3. Li, Z.S.; Feng, J.Y.; Yan, S.C.; Zou, Z. Solar fuel production: Strategies and new opportunities with nanostructures. *Nano Today* **2015**, *10*, 468–486. [CrossRef]
4. Cook, T.R.; Dogutan, D.K.; Reece, S.Y.; Surendranath, Y.; Teets, T.S.; Nocera, D.G. Solar energy supply and storage for the legacy and nonlegacy worlds. *Chem. Rev.* **2010**, *110*, 6474–6502. [CrossRef] [PubMed]
5. Jaramillo, T.F.; Jorgensen, K.P.; Bonde, J.; Nielsen, J.H.; Horch, S.; Chorkendorff, I. Identification of active edge sites for electrochemical H_2 evolution from MoS_2 nanocatalysts. *Science* **2007**, *317*, 100–102. [CrossRef] [PubMed]
6. Li, Y.G.; Wang, H.L.; Xie, L.M.; Liang, Y.Y.; Hong, G.S.; Dai, H.J. MoS_2 nanoparticles grown on graphene: An advanced catalyst for the hydrogen evolution reaction. *J. Am. Chem. Soc.* **2011**, *133*, 7296–7299. [CrossRef] [PubMed]

7. Jia, G.; Hu, Y.F.; Qian, Q.F.; Yao, Y.F.; Zhang, S.Y.; Li, Z.S.; Zou, Z.G. Formation of hierarchical structure composed of (Co/Ni)Mn-LDH nanosheets on MWCNT backbones for efficient electrocatalytic water oxidation. *ACS Appl. Mater. Interfaces* **2016**, *8*, 14527–14534. [CrossRef] [PubMed]
8. Xie, J.F.; Zhang, H.; Li, S.; Wang, R.X.; Sun, X.; Zhou, M.; Zhou, J.F.; Lou, X.W.; Xie, Y. Defect-rich MoS_2 ultrathin nanosheets with additional active edge sites for enhanced electrocatalytic hydrogen evolution. *Adv. Mater.* **2013**, *25*, 5807–5813. [CrossRef] [PubMed]
9. Lukowski, M.A.; Daniel, A.S.; Meng, F.; Forticaux, A.; Li, L.S.; Jin, S. Enhanced hydrogen evolution catalysis from chemically exfoliated metallic MoS_2 nanosheets. *J. Am. Chem. Soc.* **2013**, *135*, 10274–10277. [CrossRef] [PubMed]
10. Oyama, S.T. Preparation and catalytic properties of transition metal carbides and nitrides. *Catal. Today* **1992**, *15*, 179–200. [CrossRef]
11. Toth, L.E. *Transition Metal Carbides and Nitrides*; Academic Press: New York, NY, USA, 1971.
12. Hwu, H.H.; Chen, J.G. Surface chemistry of transition metal carbides. *Chem. Rev.* **2005**, *105*, 185–212. [CrossRef] [PubMed]
13. Kelly, T.G.; Chen, J.G. Metal overlayer on metal carbide substrate: Unique bimetallic properties for catalysis and electrocatalysis. *Chem. Soc. Rev.* **2012**, *41*, 8021–8034. [CrossRef] [PubMed]
14. Liu, P.; Rodriguez, J.A. Effects of carbon on the stability and chemical performance of transition metal carbides: A density functional study. *J. Chem. Phy.* **2004**, *120*, 5414–5423. [CrossRef] [PubMed]
15. Vrubel, H.; Hu, X.L. Molybdenum boride and carbide catalyze hydrogen evolution in both acidic and basic solutions. *Angew. Chem.* **2012**, *124*, 12875–12878. [CrossRef]
16. Hunt, S.T.; Milina, M.; Alba-Rubio, A.C.; Hendon, C.H.; Dumesic, J.A.; Roman-Leshkov, Y. Self-assembly of noble metal monolayers on transition metal carbide nanoparticle catalysts. *Science* **2016**, *352*, 974–978. [CrossRef] [PubMed]
17. Ma, F.X.; Wu, H.B.; Xia, B.Y.; Xu, C.Y.; Lou, X.W. Hierarchical beta-Mo_2C nanotubes organized by ultrathin nanosheets as a highly efficient electrocatalyst for hydrogen production. *Angew. Chem. Int. Ed.* **2015**, *54*, 15395–15399. [CrossRef] [PubMed]
18. Chen, W.F.; Wang, C.H.; Sasaki, K.; Marinkovic, N.; Xu, W.; Muckerman, J.T.; Zhu, Y.; Adzic, R.R. Highly active and durable nanostructured molybdenum carbide electrocatalysts for hydrogen production. *Energy Environ. Sci.* **2013**, *6*, 943–951. [CrossRef]
19. Hunt, S.T.; Nimmanwudipong, T.; Roman-Leshkov, Y. Engineering non–sintered, metal-terminated tungsten carbide nanoparticles for catalysis. *Angew. Chem. Int. Ed.* **2014**, *53*, 5131–5136.
20. Wan, C.; Knight, N.A.; Leonard, B.M. Crystal structure and morphology control of molybdenum carbide nanomaterials synthesized from an amine-metal oxide composite. *Chem. Commun.* **2013**, *49*, 10409–10411. [CrossRef] [PubMed]
21. Wan, C.; Regmi, Y.N.; Leonard, B.M. Multiple phases of molybdenum carbide as electrocatalysts for the hydrogen evolution reaction. *Angew. Chem.* **2014**, *126*, 6525–6528. [CrossRef]
22. Woo, Y.C.; Kang, H.J.; Kim, D.J. Formation of TiC particle during carbothermal reduction of TiO_2. *J. Eur. Ceram. Soc.* **2007**, *27*, 719–722. [CrossRef]
23. Gogotsi, Y. Chemical vapour deposition: Transition metal carbides go 2D. *Nat. Mater.* **2015**, *14*, 1079–1080. [CrossRef] [PubMed]
24. Tsuchida, T.; Kakuta, T. MA-SHS of NbC and NbB_2 in air from the Nb/B/C powder mixtures. *J. Eur. Ceram. Soc.* **2007**, *27*, 527–530. [CrossRef]
25. Vallance, S.R.; Kingman, S.; Gregory, D.H. Ultra-rapid processing of refractory carbides; 20 s synthesis of molybdenum carbide, Mo_2C. *Chem. Commun.* **2007**, *38*, 742–744. [CrossRef] [PubMed]
26. Tao, Q.; Zheng, D.F.; Zhao, X.P.; Chen, Y.L.; Li, Q.; Li, Q.; Wang, C.C.; Cui, T.; Ma, Y.M.; Wang, X.; et al. Exploring Hardness and the Distorted sp^2 Hybridization of B–B Bonds in WB_3. *Chem. Mater.* **2014**, *26*, 5297–5302. [CrossRef]
27. Luo, Y.B.; Yang, J.Y.; Li, G.; Liu, M.; Xiao, Y.; Fu, L.W.; Li, W.X.; Zhu, P.W.; Peng, J.Y.; Gao, S.; et al. Enhancement of the Thermoelectric Performance of Polycrystalline $In_4Se_{2.5}$ by Copper Intercalation and Bromine Substitution. *Adv. Energy Mater.* **2014**, *4*, 1300599. [CrossRef]
28. Tao, Q.; Zhao, X.P.; Chen, Y.L.; Li, J.; Li, Q.; Ma, Y.M.; Li, J.J.; Cui, T.; Zhu, P.W.; Wang, X. Enhanced Vickers hardness by quasi-3D boron network in MoB_2. *RSC Adv.* **2013**, *3*, 18317–18322. [CrossRef]

29. Ma, S.L.; Bao, K.; Tao, Q.; Huang, X.L.; Zhu, P.W.; Cui, T. An ultra-incompressible ternary transition metal carbide. *RSC Adv.* **2014**, *4*, 63544–63548. [CrossRef]
30. Xiao, P.; Ge, X.M.; Wang, H.B.; Liu, Z.L.; Fisher, A.; Wang, X. Novel Molybdenum carbide-tungsten carbide composite nanowires and their electrochemical activation for efficient and stable hydrogen evolution. *Adv. Funct. Mater.* **2015**, *25*, 1520–1526. [CrossRef]
31. Liu, Q.; Tian, J.Q.; Cui, W.; Jiang, P.; Cheng, N.Y.; Asiri, A.M.; Sun, X.P. Carbon nanotubes decorated with CoP nanocrystals: A highly active non-noble-metal nanohybrid electrocatalyst for hydrogen evolution. *Angew. Chem.* **2014**, *126*, 6828–6832. [CrossRef]
32. Kong, D.S.; Wang, H.T.; Lu, Z.Y.; Cui, Y. $CoSe_2$ nanoparticles grown on carbon fiber paper: An efficient and stable electrocatalyst for hydrogen evolution reaction. *J. Am. Chem. Soc.* **2014**, *136*, 4897–4900. [CrossRef] [PubMed]
33. Shi, Y.M.; Xu, Y.; Zhuo, S.F.; Zhang, J.F.; Zhang, B. Ni_2P nanosheets/Ni foam composite electrode for long-lived and pH-tolerable electrochemical hydrogen generation. *ACS Appl. Mater. Interfaces* **2015**, *7*, 2376–2384. [CrossRef] [PubMed]
34. Wang, X.; Kolen'ko, Y.V.; Bao, X.Q.; Kovnir, K.; Liu, L. One-step synthesis of self-supported nickel phosphide nanosheet array cathodes for efficient electrocatalytic hydrogen generation. *Angew. Chem. Int. Ed.* **2015**, *54*, 8188–8192. [CrossRef] [PubMed]
35. Jiang, P.; Liu, Q.; Ge, C.J.; Cui, W.; Pu, Z.H.; Asiri, A.M.; Sun, X.P. CoP nanostructures with different morphologies: Synthesis, characterization and a study of their electrocatalytic performance toward the hydrogen evolution reaction. *J. Mater. Chem. A* **2014**, *2*, 14634–14640. [CrossRef]
36. Xu, Y.F.; Gao, M.R.; Zheng, Y.R.; Jiang, J.; Yu, S.H. Nickel/Nickel(II) Oxide Nanoparticles Anchored onto Cobalt(IV) Diselenide Nanobelts for the Electrochemical Production of Hydrogen. *Angew. Chem. Int. Ed.* **2013**, *52*, 8546–8550. [CrossRef] [PubMed]

© 2016 by the authors; licensee MDPI, Basel, Switzerland. This article is an open access article distributed under the terms and conditions of the Creative Commons Attribution (CC-BY) license (http://creativecommons.org/licenses/by/4.0/).